

# Antimatter ${}^4_{\Lambda}\text{H}$ Hypernucleus Production and the ${}^3_{\Lambda}\text{H}/{}^3\text{He}$ Puzzle in Relativistic Heavy-Ion Collisions

Kai-Jia Sun<sup>1</sup> and Lie-Wen Chen<sup>\*1,2</sup>

<sup>1</sup>*Department of Physics and Astronomy and Shanghai Key Laboratory for Particle Physics and Cosmology, Shanghai Jiao Tong University, Shanghai 200240, China*

<sup>2</sup>*Center of Theoretical Nuclear Physics, National Laboratory of Heavy Ion Accelerator, Lanzhou 730000, China*

(Dated: June 21, 2016)

We show that the measured yield ratio  ${}^3_{\Lambda}\text{H}/{}^3\text{He}$  ( ${}^3_{\Lambda}\overline{\text{H}}/{}^3\overline{\text{He}}$ ) in Au+Au collisions at  $\sqrt{s_{NN}} = 200$  GeV and in Pb+Pb collisions at  $\sqrt{s_{NN}} = 2.76$  TeV can be understood within a covariant coalescence model if (anti-) $\Lambda$  particles freeze out earlier than (anti-)nucleons but their relative freezeout time is closer at  $\sqrt{s_{NN}} = 2.76$  TeV than at  $\sqrt{s_{NN}} = 200$  GeV. The earlier (anti-) $\Lambda$  freezeout can significantly enhance the yield of (anti)hypernucleus  ${}^4_{\Lambda}\text{H}$  ( ${}^4_{\Lambda}\overline{\text{H}}$ ), leading to that  ${}^4_{\Lambda}\overline{\text{H}}$  has a comparable abundance with  ${}^4\overline{\text{He}}$  and thus provides an easily measured antimatter candidate heavier than  ${}^4\overline{\text{He}}$ . The future measurement on  ${}^4_{\Lambda}\text{H}$  ( ${}^4_{\Lambda}\overline{\text{H}}$ ) would be very useful to understand the (anti-) $\Lambda$  freezeout dynamics and the production mechanism of (anti)hypernuclei in relativistic heavy-ion collisions.

PACS numbers: 25.75.-q, 25.75.Dw, 21.80.+a

*1. Introduction.*—The recent observations of light antinuclei in relativistic heavy-ion collisions at the Relativistic Heavy-Ion Collider (RHIC) [1, 2] and Large Hadron Collider (LHC) [3, 4] attract strong interest on the study of antimatter [5], and verify the general principles of quantum field theory which requires that each particle has its corresponding antiparticle and any physical system has an antimatter analog with an identical mass (but the opposite charge). These studies also provide the possibility in laboratories to test the fundamental CPT theorem [6], to explore the interactions between antimatter and antimatter [7], and to help hunting for antimatter and dark matter in the Universe through cosmic radiation observations [8]. The antihelium-4 ( ${}^4\overline{\text{He}}$  or  $\overline{\alpha}$ ) is the heaviest antimatter nucleus observed so far [2], and it is of great interest to search for antimatter nuclei heavier than  ${}^4\overline{\text{He}}$  in heavy-ion collisions, which is extremely useful to understand the production mechanism of heavier antimatter [9, 10].

Collisions of heavy nuclei at high energies also provide an abundant source of (anti)strangeness [11] and a unique tool to produce light (anti-)hypernuclei [12]. The STAR collaboration at RHIC reported the observation of hypertriton ( ${}^3_{\Lambda}\text{H}$ ) and antihypertriton ( ${}^3_{\Lambda}\overline{\text{H}}$ ) in Au+Au collisions at  $\sqrt{s_{NN}} = 200$  GeV [13], and recently the ALICE collaboration at LHC also reported the observation in Pb+Pb collisions at  $\sqrt{s_{NN}} = 2.76$  TeV [14]. The value of measured yield ratio  ${}^3_{\Lambda}\text{H}/{}^3\text{He}$  is  $0.82 \pm 0.16(\text{stat.}) \pm 0.12(\text{syst.})$  for 0–80% centrality Au+Au collisions at  $\sqrt{s_{NN}} = 200$  GeV (RHIC) [13] and  $0.47 \pm 0.10(\text{stat.}) \pm 0.13(\text{syst.})$  in central (0–10% centrality) Pb+Pb collisions at  $\sqrt{s_{NN}} = 2.76$  TeV (LHC) [14].

It is thus favored that the measured  ${}^3_{\Lambda}\text{H}/{}^3\text{He}$  ratio at RHIC is higher than that at LHC, although they are compatible with a very small overlap within the uncertainties by combing the statistical and systematic uncertainties, i.e.,  $0.82 \pm 0.20$  at RHIC and  $0.47 \pm 0.16$  at LHC. The value of the  ${}^3_{\Lambda}\text{H}/{}^3\text{He}$  ratio for 0–80% centrality at RHIC (i.e.,  $0.82 \pm 0.20$ ) is expected to be further enhanced for central collisions since the ALICE measurements indicate that the  ${}^3_{\Lambda}\text{H}/{}^3\text{He}$  ratio in central Pb+Pb collisions is higher than that in peripheral Pb+Pb collisions [14]. Similar conclusion is obtained for the  ${}^3_{\Lambda}\overline{\text{H}}/{}^3\overline{\text{He}}$  ratio for which the measured value is  $0.89 \pm 0.28(\text{stat.}) \pm 0.13(\text{syst.})$  for 0–80% centrality Au+Au collisions at  $\sqrt{s_{NN}} = 200$  GeV [13] and  $0.42 \pm 0.10(\text{stat.}) \pm 0.13(\text{syst.})$  in central (0–10% centrality) Pb+Pb collisions at  $\sqrt{s_{NN}} = 2.76$  TeV [14]. As shown in Ref. [14], the conventional (statistical) thermal models [15–18] failed to describe the RHIC ratio, although some of them [15–17] successfully described the LHC ratio. The thermal model with a multi-freezeout configuration [19] reasonably described the ratio at RHIC but failed at LHC, and so did the parton and hadron cascade plus dynamically constrained phase-space coalescence model [20, 21]. The dynamical [22] and simple [23, 24] coalescence models described marginally the ratio at RHIC but no results are available at LHC. Therefore, the measured  ${}^3_{\Lambda}\text{H}/{}^3\text{He}$  and  ${}^3_{\Lambda}\overline{\text{H}}/{}^3\overline{\text{He}}$  ratios challenge all theoretical calculations performed so far and call for novel mechanisms for (anti-)hypernuclei production in these collisions.

Since hyperons have quite different interactions compared with nucleons [25], they are expected to have different freezeout dynamics in heavy-ion collisions, which will lead to distinct features for the production of light (anti)hypernuclei compared with that of light normal (anti)nuclei. In this work, we show that the covariant coalescence model can naturally reproduce the measured

\*Corresponding author (email: lwchen@sjtu.edu.cn)

${}^3_{\Lambda}\text{H}/{}^3\text{He}$  ( ${}^3_{\Lambda}\overline{\text{H}}/{}^3\overline{\text{He}}$ ) at both RHIC and LHC if (anti-) $\Lambda$  particles freeze out earlier than (anti)nucleons but their relative freezeout time is closer at LHC than at RHIC. The earlier anti- $\Lambda$  ( $\overline{\Lambda}$ ) freezeout leads to that the heavier antihypernucleus  ${}^4_{\Lambda}\overline{\text{H}}$  has a comparable yield with  ${}^4\overline{\text{He}}$  and thus provides an easily measured candidate for anti-matter heavier than  ${}^4\overline{\text{He}}$ .

2. *Covariant coalescence model.*—We use the covariant coalescence model [26] for the production of light clusters in heavy-ion collisions. The main feature of the coalescence model [27–29] is that the coalescence probability depends on the details of the phase space structure of the constituent particles at freezeout as well as the statistical weight and internal structure (wave function) of the coalesced cluster, and these details are of no relevance in the thermal model [15, 16, 30–32] of cluster creation.

The phase space configuration of the constituent particles at freezeout is a basic ingredient in the coalescence model, and in principle it can be obtained dynamically from transport model simulations for heavy-ion collisions (see, e.g., Refs. [33–37]). For the particle production at mid-rapidity in central heavy-ion collisions at RHIC and LHC considered here, for simplicity, we assume a boost-invariant longitudinal expansion for the constituent particles which are emitted from a freezeout hypersurface  $\Sigma^\mu$ , and the Lorentz invariant one-particle momentum distribution is then given by

$$E \frac{d^3N}{d^3p} = \frac{d^3N}{p_T dp_T d\phi_p dy} = \int_{\Sigma^\mu} d\sigma_\mu p^\mu f(x, p) = \int d^4x S(x, p), \quad (1)$$

where  $\sigma_\mu$  denotes the normal vector of hypersurface  $\Sigma^\mu$  and  $p^\mu$  is the four-momentum of the emitted particle. The emission function  $S(x, p)$  can be expressed by

$$S(x, p) d^4x = m_T \cosh(\eta - y) f(x, p) J(\tau) \tau d\tau d\eta r dr d\phi_s, \quad (2)$$

where we use longitudinal proper time  $\tau = \sqrt{t^2 - z^2}$ , spacetime rapidity  $\eta = \frac{1}{2} \ln \frac{t+z}{t-z}$ , cylindrical coordinates  $(r, \phi_s)$ , rapidity  $y = \frac{1}{2} \ln \frac{E+p_z}{E-p_z}$ , transverse momentum  $(p_T, \phi_p)$ , and transverse mass  $m_T = \sqrt{m^2 + p_T^2}$ . The statistical distribution function  $f(x, p)$  is given by  $f(x, p) = g(2\pi)^{-3} [\exp(p^\mu u_\mu / kT) / \xi \pm 1]^{-1}$  with  $g$  being spin degeneracy factor,  $\xi$  the fugacity,  $u_\mu$  the four-velocity of a fluid element in the fireball,  $T$  the local temperature, and  $p^\mu u_\mu = m_T \cosh \rho \cosh(\eta - y) - p_T \sinh \rho \cos(\phi_p - \phi_s)$  the energy in local rest frame of the fluid. Following Ref. [38], we assume the freezeout time follows a Gaussian distribution  $J(\tau) = \frac{1}{\Delta\tau\sqrt{2\pi}} \exp(-\frac{(\tau-\tau_0)^2}{2(\Delta\tau)^2})$  with a mean value  $\tau_0$  and a dispersion  $\Delta\tau$ , and the transverse rapidity distribution of the fluid element in the fireball is parameterized as  $\rho = \rho_0 r / R_0$  with  $\rho_0$  being the maximum transverse rapidity and  $R_0$  the transverse radius of the fireball. The phase space freezeout configuration of the constituent particles is thus determined by six parameters, i.e.,  $T$ ,  $\rho_0$ ,  $R_0$ ,  $\tau_0$ ,  $\Delta\tau$  and  $\xi$ .

The cluster production probability is determined by the overlap of the cluster Wigner function with the constituent particle phase-space distribution at freezeout. If

$M$  particles are coalesced into a cluster, the invariant momentum distribution of the cluster can be obtained as

$$E \frac{d^3N_c}{d^3P} = E g_c \int \left( \prod_{i=1}^M \frac{d^3p_i}{E_i} d^4x_i S(x_i, p_i) \right) \times \rho_c^W(x_1, \dots, x_M; p_1, \dots, p_M) \delta^3(\mathbf{P} - \sum_{i=1}^M \mathbf{p}_i) \quad (3)$$

where  $N_c$  is the cluster multiplicity,  $E(\mathbf{P})$  is its energy (momentum),  $g_c$  is the coalescence factor, and  $\rho_c^W$  is the Wigner function. In this work, the harmonic oscillator wave functions are assumed for all the clusters in the rest frame except the (anti)deutrons for which the Hulthén wave function is used (see, e.g., Refs. [33, 34]), and so the cluster Wigner functions and root-mean-square radii  $r_{\text{rms}}$  can be obtained analytically. The details about how to calculate the integral (3) can be found in Ref. [10]. It should be stressed that since the constituent particles may have different freezeout time, the particles that freeze out earlier are allowed to propagate freely until the time when the last particles in the cluster freezes out to make the coalescence at equal time [10, 33, 35].

3. *Production of (anti)hypertriton.*—The coalescence factor is given by  $g_c = \frac{2^{j+1}}{2^N}$  [28] with  $j$  the spin and  $N$  the nucleon number of the nucleus. For d,  ${}^3\text{He}$ ,  ${}^3_{\Lambda}\text{H}$ ,  ${}^4\text{He}$  and  ${}^4_{\Lambda}\text{H}$  that we focus on here, their spins are 1, 1/2, 1/2, 0 and 0, respectively, and their  $r_{\text{rms}}$  which are directly related to their Wigner functions [10], are 1.96 fm, 1.76 fm, 4.9 fm, 1.45 fm and 2.0 fm, respectively [39, 40]. The anti(hyper)nuclei are assumed to have the same  $j$  and  $r_{\text{rms}}$  as their corresponding (hyper)nuclei.

Following Ref. [10], the proton (p) freezeout parameters  $T$  and  $\rho_0$  can be extracted from fitting the p spectrum, and the  $R_0$ ,  $\tau_0$ ,  $\Delta\tau$  and  $\xi_p$  can be obtained by further fitting the spectra of d and  ${}^3\text{He}$  in the coalescence model. For central Au+Au collisions at  $\sqrt{s_{NN}} = 200$  GeV, we obtain  $T = 111.6$  MeV,  $\rho_0 = 0.98$ ,  $R_0 = 15.6$  fm,  $\tau_0 = 10.6$  fm/c,  $\Delta\tau = 3.5$  fm/c and  $\xi_p = 10.5$  by fitting the p spectrum from PHENIX [41] and the spectra of d and  ${}^3\text{He}$  from STAR [1], and for antiprotons ( $\overline{p}$ ), we assume they have the same freezeout as protons except the fugacity is reduced to  $\xi_{\overline{p}} = 7.84$  to describe the measured  $\overline{p}/p = 0.75$  [41]. For central Pb+Pb collisions at  $\sqrt{s_{NN}} = 2.76$  TeV, we obtain  $T = 121.1$  MeV,  $\rho_0 = 1.215$ ,  $R_0 = 19.7$  fm,  $\tau_0 = 15.5$  fm/c,  $\Delta\tau = 1.0$  fm/c and  $\xi_p = 3.72$  by fitting the measured spectra of p, d,  ${}^3\text{He}$  from ALICE [1, 4, 42], and the antiprotons are assumed to have the same freezeout parameters as protons since the  $\overline{p}/p$  is close to unity at LHC. For neutrons (n) (antineutrons ( $\overline{n}$ )), we take their freezeout parameters as those of p's ( $\overline{p}$ 's) since the isospin chemical potential at freezeout is small at RHIC and LHC [15]. The p freezeout parameters at RHIC (denoted by FOAu-N) and LHC (denoted by FOPb-N) are summarized in Table I, and the freezeout hypersurface at LHC is seen to have larger  $T$ ,  $\rho_0$ ,  $R_0$  and  $\tau_0$  but smaller  $\Delta\tau$  and  $\xi_p$ . In Fig. 1, the experimental data are compared with the calculated re-

TABLE I: Parameters of various freezeout configurations for (anti)nucleons and (anti-) $\Lambda$  particles at midrapidity in central collisions of Au+Au at  $\sqrt{s_{NN}} = 200$  GeV (FOAu) and Pb+Pb at  $\sqrt{s_{NN}} = 2.76$  TeV (FOPb). The unit of  $\tau_0$  and  $\Delta\tau$  is fm/c.  $\xi$  and  $\bar{\xi}$  denote the fugacity of particles and antiparticles, respectively.

	$T$ (MeV)	$\rho_0$	$R_0$ (fm)	$\tau_0$	$\Delta\tau$	$\xi$	$\bar{\xi}$
FOAu-N	111.6	0.980	15.6	10.6	3.5	10.5	7.84
FOPb-N	121.1	1.215	19.7	15.5	1.0	3.72	3.72
FOAu- $\Lambda$	111.6	0.980	15.6	10.6	3.5	42.8	35.1
FOPb- $\Lambda$	121.1	1.215	19.7	15.5	1.0	9.54	9.54
FOAu- $\Lambda^*$	126.0	0.890	11.1	7.54	3.5	35.1	28.8
FOPb- $\Lambda^*$	123.4	1.171	16.7	13.1	1.0	13.6	13.6

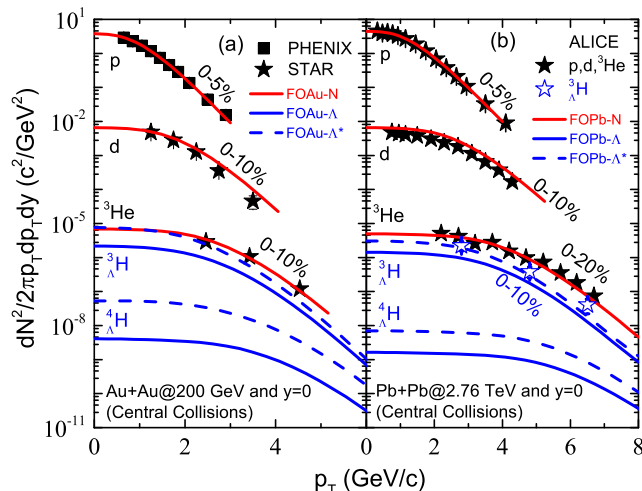


FIG. 1: Transverse momentum distributions of p, d,  ${}^3\text{He}$ ,  ${}^3_\Lambda\text{H}$  and  ${}^4_\Lambda\text{H}$  at midrapidity in central collisions of Au+Au at  $\sqrt{s_{NN}} = 200$  GeV (a) and Pb+Pb at  $\sqrt{s_{NN}} = 2.76$  TeV (b) predicted by coalescence model with various freezeout configurations. For Au+Au collisions, the data of proton is taken from the PHENIX [41] and those of d and  ${}^3\text{He}$  are taken from STAR [1]. The data of p, d,  ${}^3\text{He}$  and  ${}^3_\Lambda\text{H}$  for Pb+Pb collisions are taken from ALICE [4, 14, 42].

results for the spectra of p, d and  ${}^3\text{He}$  with FOAu-N and FOPb-N, and one can see that the coalescence model describes well the measured spectra. Table II lists the  $p_T$ -integrated yield in the midrapidity region ( $-0.5 \leq y \leq 0.5$ ) (i.e.,  $dN/dy$ ) for p ( $\bar{p}$ ), d ( $\bar{d}$ ),  ${}^3\text{He}$  ( ${}^3\bar{\text{He}}$ ) and  ${}^4\text{He}$  ( ${}^4\bar{\text{He}}$ ) with FOAu-N and FOPb-N, and it is seen that the  $dN/dy$  values of d,  ${}^3\text{He}$  and  ${}^4\text{He}$  ( $\bar{d}$ ,  ${}^3\bar{\text{He}}$  and  ${}^4\bar{\text{He}}$ ) at LHC are roughly two (four) times as large as those at RHIC.

For  $\Lambda$  particles, we first assume they have the same freezeout configuration as nucleons except that the  $\Lambda$  fugacity becomes  $\xi_\Lambda = 42.8$  (9.54) at RHIC (LHC) by fitting the experimental  $\Lambda$  spectra [43, 44] as shown in Fig. 2 by solid lines. The  $\bar{\Lambda}$  particles are assumed to have the same freezeout parameters as  $\Lambda$  particles except the fugacity at RHIC is reduced to  $\xi_{\bar{\Lambda}} = 35.1$  to describe the measured  $\bar{\Lambda}/\Lambda = 0.82$  [43]. The (anti-) $\Lambda$  freezeout pa-

TABLE II:  $dN/dy$  at midrapidity of light (anti)(hyper)hypernuclei for various freezeout configurations in central collisions of Au+Au at  $\sqrt{s_{NN}} = 200$  GeV (FOAu) and Pb+Pb at  $\sqrt{s_{NN}} = 2.76$  TeV (FOPb).

	p( $\bar{p}$ )	d( $\bar{d}$ )	${}^3\text{He}$ ( ${}^3\bar{\text{He}}$ )	${}^4\text{He}$ ( ${}^4\bar{\text{He}}$ )
FOAu-N	16.1(12.1)	$7.49(4.21) \times 10^{-2}$	$14.9(6.29) \times 10^{-5}$	$15.4(4.88) \times 10^{-8}$
FOPb-N	33.5(33.5)	$15.0(15.0) \times 10^{-2}$	$2.36(2.36) \times 10^{-4}$	$2.20(2.20) \times 10^{-7}$
	$\Lambda$ ( $\bar{\Lambda}$ )		${}^3_\Lambda\text{H}$ ( ${}^3_\Lambda\bar{\text{H}}$ )	${}^4_\Lambda\text{H}$ ( ${}^4_\Lambda\bar{\text{H}}$ )
FOAu- $\Lambda$	17.0(14.0)		$4.26(1.96) \times 10^{-5}$	$14.8(5.12) \times 10^{-8}$
FOPb- $\Lambda$	24.9(24.9)		$5.72(5.72) \times 10^{-5}$	$1.36(1.36) \times 10^{-7}$
FOAu- $\Lambda^*$	18.8(15.4)		$12.3(5.65) \times 10^{-5}$	$15.7(5.43) \times 10^{-7}$
FOPb- $\Lambda^*$	25.9(25.9)		$1.12(1.12) \times 10^{-4}$	$5.43(5.43) \times 10^{-7}$

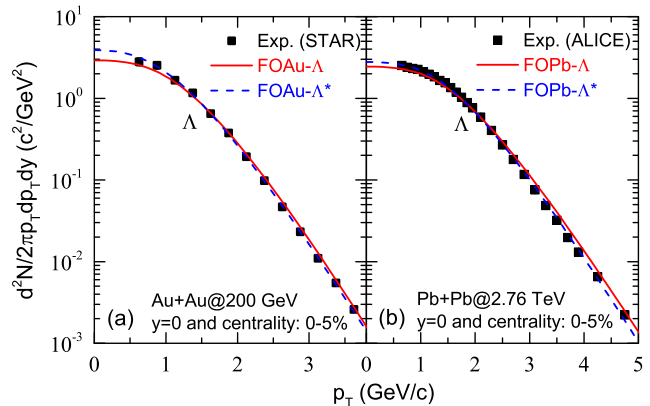


FIG. 2: Transverse momentum distribution of  $\Lambda$ 's in central collisions of Au+Au at  $\sqrt{s_{NN}} = 200$  GeV (a) and Pb+Pb at  $\sqrt{s_{NN}} = 2.76$  TeV (b) from coalescence model calculations with various freezeout configurations. The experimental data are taken from STAR [43] for the Au+Au collisions and from ALICE [44] for the Pb+Pb collisions.

rameters are listed as FOAu- $\Lambda$  (FOPb- $\Lambda$ ) in Table I for the central Au+Au (Pb+Pb) collisions. With FOAu- $\Lambda$  and FOPb- $\Lambda$  (together with FOAu-N and FOPb-N), the spectra of  ${}^3_\Lambda\text{H}$  and  ${}^4_\Lambda\text{H}$  can then be calculated using the coalescence model, and the results are shown in Fig. 1. The  $dN/dy$  values for  $\Lambda$  ( $\bar{\Lambda}$ ),  ${}^3_\Lambda\text{H}$  ( ${}^3_\Lambda\bar{\text{H}}$ ) and  ${}^4_\Lambda\text{H}$  ( ${}^4_\Lambda\bar{\text{H}}$ ) are summarized in Table II, and the resulting  ${}^3_\Lambda\text{H}/{}^3\text{He}$  is about 0.29 (0.24) at RHIC (LHC) with FOAu- $\Lambda$  (FOPb- $\Lambda$ ), which significantly underestimates the measured values from STAR [13] and ALICE [14], i.e.,  $0.82 \pm 0.16(\text{stat.}) \pm 0.12(\text{syst.})$  for 0 – 80% centrality Au+Au collisions at  $\sqrt{s_{NN}} = 200$  GeV [13] and  $0.47 \pm 0.10(\text{stat.}) \pm 0.13(\text{syst.})$  in central (0 – 10% centrality) Pb+Pb collisions at  $\sqrt{s_{NN}} = 2.76$  TeV [14]. The predicted ratio  ${}^3_\Lambda\text{H}/{}^3\text{He}$  is about 0.31 (0.24) at RHIC (LHC) with FOAu- $\Lambda$  (FOPb- $\Lambda$ ), again significantly underestimating the measured values, i.e.,  $0.89 \pm 0.28(\text{stat.}) \pm 0.13(\text{syst.})$  from STAR [13] and  $0.42 \pm 0.10(\text{stat.}) \pm 0.13(\text{syst.})$  from ALICE [14]. In addition, the predicted  ${}^3_\Lambda\text{H}$  spectrum with FOPb- $\Lambda$  is seen to underestimate the recently measured spectrum by ALICE [14].

To understand the disagreement of  ${}^3_\Lambda\text{H}/{}^3\text{He}$  ( ${}^3_\Lambda\bar{\text{H}}/{}^3\bar{\text{He}}$ )

and the  ${}^3_{\Lambda}\text{H}$  spectrum between the predictions and the measurements, we extract the  $\Lambda$  freezeout parameters  $T$  and  $\rho_0$  by directly fitting the measured  $\Lambda$  spectra [43, 44] as shown in Fig 2 by dashed lines, and we obtain  $T = 126$  (123.4) MeV and  $\rho_0 = 0.89$  (1.171) for Au+Au (Pb+Pb) collisions, which better describe the data than FOAu- $\Lambda$  (FOPb- $\Lambda$ ). The  $\Lambda$  particles thus have a higher freezeout temperature than nucleons, especially at RHIC, implying an earlier freezeout for  $\Lambda$  particles than for nucleons, which is consistent with the empirical picture that the strange baryons usually freeze out earlier than the nonstrange baryons due to their relatively smaller interaction cross sections. The earlier  $\Lambda$  freezeout is also supported by the investigation on strangeness production [19, 45–48] as well as the microscopic transport model simulations [49].

An earlier  $\Lambda$  freezeout means the  $\Lambda$  particles can pick up unfrozen-out nucleons to form light hypernuclei, and this implies the nucleons coalesced into light hypernuclei also have an earlier freezeout time than those coalesced into normal light nuclei. To consider this effect, for the coalescence production of light hypernuclei, we reduce the  $\tau_0$  and  $R_0$  simultaneously but increase the  $\xi$  to fit the  $\Lambda$  and p spectra. In this way, the earlier freezeout increases the phase space density of  $\Lambda$ , p and n, and thus the  ${}^3_{\Lambda}\text{H}$  production rate. To fit the measured central value 0.82 (0.47) of the  ${}^3_{\Lambda}\text{H}/{}^3\text{He}$  ratio at RHIC (LHC), we find the  $R_0$  and  $\tau_0$  need to be reduced to 71% (85%) of their values in FOAu- $\Lambda$  (FOPb- $\Lambda$ ), i.e.,  $R_0 = 11.1$  (16.7) fm and  $\tau_0 = 7.54$  (13.1) fm/c, if we fix  $T = 126$  (123.4) MeV,  $\rho_0 = 0.89$  (1.171) and  $\Delta\tau = 3.5$  (1.0) fm/c. These new freezeout configurations are denoted as FOAu- $\Lambda^*$  and FOPb- $\Lambda^*$  in Table I. It is interesting to note that the  $\Lambda$  freezeout temperature is slightly higher at RHIC than at LHC. For FOAu- $\Lambda^*$  and FOPb- $\Lambda^*$ , we have neglected final state interactions of the produced  ${}^3_{\Lambda}\text{H}$  during the last 2 ~ 3 fm/c time interval when some nucleons have not yet frozen out, and probably this can be justified from the transport model study which indicates including the final state interactions changes the deuteron yield by only about 20% at RHIC [36]. On the other hand, since  ${}^3_{\Lambda}\text{H}$  is an even more loosely bound system than deuteron (Note the total binding energy of  ${}^3_{\Lambda}\text{H}$  is 2.354 MeV with the  $\Lambda$  separation energy of only about 0.13 MeV [50], and the total binding energy of deuteron is 2.224 MeV [51]), the effects of the final state interactions on  ${}^3_{\Lambda}\text{H}$  yield are thus expected to be stronger than that on deuteron. For  ${}^4_{\Lambda}\text{H}$ , the total binding energy is 10.601 MeV with the  $\Lambda$  separation energy of 2.12 MeV [52], and the effects of the final state interactions are thus expected to be similar with the case of deuteron. The quantitative information on the final interaction effects needs a complicated transport model simulations. The stronger final state interaction (destruction) of  ${}^3_{\Lambda}\text{H}$  implies the  $\Lambda$  particles need an even earlier freezeout than that obtained above, and the effects of an earlier  $\Lambda$  freezeout in the present work are thus considered to be conservative estimate.

The predicted spectra of  ${}^3_{\Lambda}\text{H}$  and  ${}^4_{\Lambda}\text{H}$  with FOAu- $\Lambda^*$

and FOPb- $\Lambda^*$  are shown in Fig. 1 by dashed lines, and one can see that compared with FOAu- $\Lambda$  and FOPb- $\Lambda$ , FOAu- $\Lambda^*$  and FOPb- $\Lambda^*$  significantly enhance the production of  ${}^3_{\Lambda}\text{H}$  and  ${}^4_{\Lambda}\text{H}$  and now the  ${}^3_{\Lambda}\text{H}$  spectra measured by ALICE [14] can be reasonably described by FOPb- $\Lambda^*$ . The  $dN/dy$  values for  $\Lambda$  ( $\bar{\Lambda}$ ),  ${}^3_{\Lambda}\text{H}$  ( ${}^3_{\Lambda}\bar{\text{H}}$ ) and  ${}^4_{\Lambda}\text{H}$  ( ${}^4_{\Lambda}\bar{\text{H}}$ ) with FOAu- $\Lambda^*$  and FOPb- $\Lambda^*$  are listed in Table II. The small difference for the  $dN/dy$  of (anti-) $\Lambda$  between FOAu- $\Lambda^*$  (FOPb- $\Lambda^*$ ) and FOAu- $\Lambda$  (FOPb- $\Lambda$ ) is due to the slight variation of the  $\Lambda$  spectra from different fits as shown in Fig 2. The calculated  ${}^3_{\Lambda}\text{H}/{}^3\text{He}$  and  ${}^3_{\Lambda}\bar{\text{H}}/{}^3\bar{\text{He}}$  ratios are, respectively, about 0.83 (0.47) and 0.91 (0.47) at RHIC (LHC) with FOAu- $\Lambda^*$  (FOPb- $\Lambda^*$ ), nicely reproducing the measured central values. Therefore, our results suggest that the (anti-) $\Lambda$  particles may freeze out earlier than (anti)nucleons but their relative freezeout time is closer at LHC than at RHIC. It is interesting to see that the  $\Lambda$  and nucleon freezeout parameters seem to come close to each other as the energy increases and this is understandable since a higher colliding energy generally leads to a longer-lived hadronic fireball where the  $\Lambda$ 's and nucleons will experience more collisions.

The ratio  $S_3 = {}^3_{\Lambda}\text{H}/({}^3\text{He}\times\Lambda/p)$  was first suggested in Ref. [53] in the expectation that dividing the strange to nonstrange baryon yield should result in a value near unity in a naive coalescence model. It was also argued [22] to be a good representation of the local correlation between baryon number and strangeness [54], and thus should be a valuable probe for the onset of deconfinement in relativistic heavy-ion collisions. The  $S_3$  was measured to be  $1.08 \pm 0.22$  for 0-80% centrality Au+Au collisions [13] and  $0.60 \pm 0.13(\text{stat.}) \pm 0.21(\text{syst.})$  for central (0-10% centrality) Pb+Pb collisions [14]. For central collisions considered here, the  $S_3$  for Au+Au (Pb+Pb) collisions is 0.27 (0.33) with FOAu- $\Lambda$  (FOPb- $\Lambda$ ), while it increases to 0.71 (0.61) with FOAu- $\Lambda^*$  (FOPb- $\Lambda^*$ ). The FOAu- $\Lambda$  (FOPb- $\Lambda$ ) thus significantly underestimates the measured  $S_3$  for Au+Au (Pb+Pb) collisions. While FOPb- $\Lambda^*$  nicely reproduces the measured  $S_3$  for Pb+Pb collisions, the FOAu- $\Lambda^*$  still underestimates the measured  $S_3$  for Au+Au collisions. It should be noted that while there is negligible feed-down from heavier states into  ${}^3_{\Lambda}\text{H}$  and  ${}^3\text{He}$ , the  $\Lambda$  and p are significantly influenced by feed-down from decays of excited baryonic states. In the coalescence model calculations, the  $\Lambda$  and p from the short-lived strong decays are included since they appear in the fireball, while those from the other long-lived decays are excluded since they are out of the fireball. In the calculation of the  $S_3$  for Au+Au collisions, we use the p spectrum from PHENIX [41] which is corrected by excluding the contribution from the long-lived weak decays. We note that including 40% contribution from weak decays to the p yield leads to  $S_3 = 0.994$  for Au+Au collisions with FOPb- $\Lambda^*$ , consistent with the measured value from STAR.

It should be pointed out that although the  $\Lambda$ 's and nucleons are assumed to have the same freezeout configuration, the  $S_3$  is still significantly less than unity (e.g.,

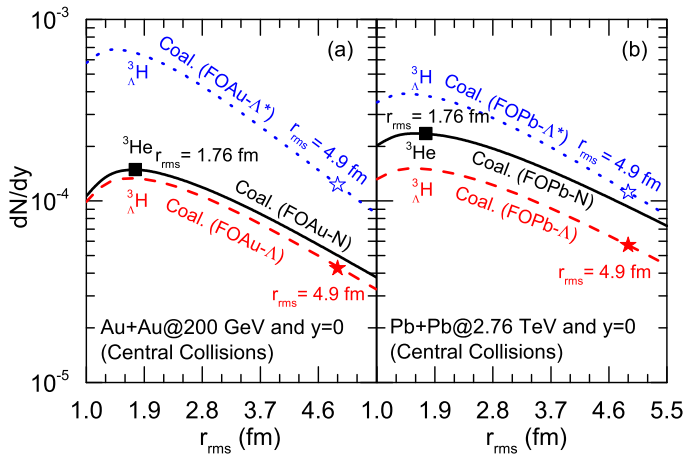


FIG. 3: The predicted  $dN/dy$  of  ${}^3_{\Lambda}\text{H}$  and  ${}^3\text{He}$  at midrapidity as a function of their root-mean-square radii  $r_{\text{rms}}$  in central collisions of Au+Au at  $\sqrt{s_{NN}} = 200$  GeV (a) and Pb+Pb at  $\sqrt{s_{NN}} = 2.76$  TeV (b) from the coalescence model with various freezeout configurations. The stars (squares) indicate the empirical size values  $r_{\text{rms}} = 4.9$  (1.76) fm for  ${}^3_{\Lambda}\text{H}$  ( ${}^3\text{He}$ ).

$S_3 = 0.27$  (0.32) for FOAu- $\Lambda$  (FOPb- $\Lambda$ ). This is mainly due to the much larger size of  ${}^3_{\Lambda}\text{H}$  than that of  ${}^3\text{He}$ , as suggested first in Ref. [53]. To see this more clearly, we show in Fig. 3 the predicted  $dN/dy$  of  ${}^3_{\Lambda}\text{H}$  and  ${}^3\text{He}$  as a function of their root-mean-square radii in central collisions of Au+Au at  $\sqrt{s_{NN}} = 200$  GeV and Pb+Pb at  $\sqrt{s_{NN}} = 2.76$  TeV from the coalescence model with various freezeout configurations. The empirical size values, i.e.,  $r_{\text{rms}} = 4.9$  fm for  ${}^3_{\Lambda}\text{H}$  and  $r_{\text{rms}} = 1.76$  fm for  ${}^3\text{He}$  are also indicated in Fig. 3. It is seen that, because of the finite size cut off effect of the fireball in the spatial part integration of Eq. (3), the  $dN/dy$  decrease with  $r_{\text{rms}}$  when  $r_{\text{rms}}$  is larger than about 1.6 fm. Furthermore, it is interesting to see that the  $dN/dy$  exhibits a stronger  $r_{\text{rms}}$  dependence at RHIC than that at LHC, and this is mainly due to the fact that the freezeout volume ( $\pi R_0^2 \tau_0$ ) is smaller at RHIC. Compared with the thermal model, the coalescence model thus has a distinct feature that the cluster yield depends on the cluster size, as mentioned earlier. Assuming  ${}^3_{\Lambda}\text{H}$  has a same  $r_{\text{rms}}$  as  ${}^3\text{He}$ , i.e.,  $r_{\text{rms}} = 1.76$  fm, we find that the  $S_3$  values for both Au+Au (with FOAu- $\Lambda$ ) and Pb+Pb (with FOPb- $\Lambda$ ) collisions are drastically enhanced to about 0.85, and further to unity if the  $\Lambda$ 's and nucleons are assumed to have equal mass, as expected from the naive coalescence model.

4. *Production of  ${}^4_{\Lambda}\text{H}$  ( ${}^4_{\Lambda}\overline{\text{H}}$ ).*—The  ${}^4_{\Lambda}\text{H}$  is a well-researched hypernucleus with lifetime of  $192^{+20}_{-18}$  ps [55] and mass  $M({}^4_{\Lambda}\text{H}) = 3922.484 \pm 0.01(\text{stat.}) \pm 0.09(\text{syst.})$  MeV [52] (Note the mass of  ${}^4\text{He}$  is  $M({}^4\text{He}) = 3727.379$  MeV). The  ${}^4_{\Lambda}\text{H}$  can be identified through the  ${}^4\text{He}-\pi^-$  invariant mass spectrum from the decay  ${}^4_{\Lambda}\text{H} \rightarrow {}^4\text{He} + \pi^-$  with branching ratio of about 50% [56, 57].

Shown in Fig. 4 are the predicted  $dN/dy$  of light (anti)(hyper)nuclei as a function of  $\frac{B}{|B|}m$ , where  $B$  is the

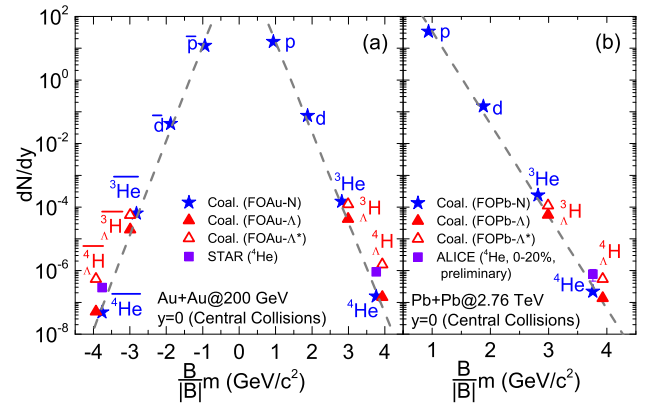


FIG. 4: The predicted  $dN/dy$  of light (anti)(hyper)nuclei at midrapidity as a function of  $\frac{B}{|B|}m$  in central collisions of Au+Au at  $\sqrt{s_{NN}} = 200$  GeV (a) and Pb+Pb at  $\sqrt{s_{NN}} = 2.76$  TeV (b) from the coalescence model with various freezeout configurations. The squares in (a) represent the results for  ${}^4\text{He}$  and  ${}^4\overline{\text{He}}$  in the Au+Au collisions by considering the binding energy effects to fit STAR data [2, 10] while the square in (b) is the preliminary result for  ${}^4\text{He}$  in 0–20% centrality Pb+Pb collisions from ALICE measurement [58].

baryon number of light clusters and  $m$  is the corresponding mass, in central collisions of Au+Au at  $\sqrt{s_{NN}} = 200$  GeV and Pb+Pb at  $\sqrt{s_{NN}} = 2.76$  TeV from the coalescence model with various freezeout configurations. For the Pb+Pb collisions, we only show the results of (hyper)nuclei in Fig. 4 because the results of anti-(hyper)nuclei are the same as those of their corresponding (hyper)nuclei since the antiprotons (and anti- $\Lambda$ 's) are assumed to have the same freezeout configuration as their corresponding particles in central Pb+Pb collisions at  $\sqrt{s_{NN}} = 2.76$  TeV. Also included in Fig. 4 are the preliminary result for  $dN/dy$  (i.e.,  $7.8 \pm 3.1 \times 10^{-7}$ ) of  ${}^4\text{He}$  in central (0–20%) Pb+Pb collisions at  $\sqrt{s_{NN}} = 2.76$  TeV recently measured by ALICE [58] as well as the results for  $dN/dy$  of  ${}^4\text{He}$  and  ${}^4\overline{\text{He}}$  in central Au+Au collisions obtained from the coalescence model by considering the binding energy effects to fit the STAR data (for details see Ref [10]). Since FOAu-N and FOPb-N describe well the spectra of p, d and  ${}^3\text{He}$  as shown in Fig. 1, the predicted  $dN/dy$  of p ( $\overline{\text{p}}$ ), d ( $\overline{\text{d}}$ ) and  ${}^3\text{He}$  ( ${}^3\overline{\text{He}}$ ) in Fig. 4 are expected to give good estimates of the experimental data on  $dN/dy$ . On the other hand, FOAu-N and FOPb-N significantly underestimate the  $dN/dy$  of  ${}^4\text{He}$  and  ${}^4\overline{\text{He}}$ , and these discrepancies can be fixed by considering the effects of the large binding energy of  ${}^4\text{He}$  and  ${}^4\overline{\text{He}}$  [10].

Furthermore, it is seen from Fig. 4 that compared with FOAu- $\Lambda$  (FOPb- $\Lambda$ ), FOAu- $\Lambda^*$  (FOPb- $\Lambda^*$ ) significantly enhances the  $dN/dy$  of (anti)- ${}^3_{\Lambda}\text{H}$  and (anti)- ${}^4_{\Lambda}\text{H}$  due to the earlier  $\Lambda$  freezeout. From the detailed numbers listed in Table II, one can see that in Au+Au collisions, the  $dN/dy$  of  ${}^4_{\Lambda}\text{H}$  ( ${}^4_{\Lambda}\overline{\text{H}}$ ) is  $1.48 \times 10^{-7}$  ( $5.12 \times 10^{-8}$ ) with FOAu- $\Lambda$  and  $1.57 \times 10^{-6}$  ( $5.43 \times 10^{-7}$ ) with FOAu- $\Lambda^*$ , implying the earlier  $\Lambda$  freezeout enhances the yields

of both  ${}^4_{\Lambda}\text{H}$  and  ${}^4_{\Lambda}\overline{\text{H}}$  by a factor of 10.6. In Pb+Pb collisions, the  $dN/dy$  of  ${}^4_{\Lambda}\text{H}$  (same for  ${}^4_{\Lambda}\overline{\text{H}}$ ) is  $1.36 \times 10^{-7}$  with FOPb- $\Lambda$  and  $5.43 \times 10^{-7}$  with FOPb- $\Lambda^*$ , and the enhancement factor due to the earlier  $\Lambda$  freezeout is 4.0. It is interesting to see that the  $dN/dy$  of  ${}^4_{\Lambda}\text{H}$  ( ${}^4_{\Lambda}\overline{\text{H}}$ ) at RHIC (with FOAu- $\Lambda^*$ ) is about 3.5(1.0) times as large as that at LHC (with FOPb- $\Lambda^*$ ), and the predicted yields of the heavier  ${}^4_{\Lambda}\text{H}$  ( ${}^4_{\Lambda}\overline{\text{H}}$ ) at RHIC are larger than the measured  ${}^4\text{He}$  ( ${}^4\overline{\text{He}}$ ) yield at RHIC (i.e., about  $9.18 \times 10^{-7}$  for  ${}^4\text{He}$  and  $2.91 \times 10^{-7}$  for  ${}^4\overline{\text{He}}$  [10]). Also the predicted  $dN/dy$  of  ${}^4_{\Lambda}\text{H}$  ( ${}^4_{\Lambda}\overline{\text{H}}$ ) with FOPb- $\Lambda^*$  at LHC (i.e.,  $5.43 \times 10^{-7}$ ) is very close to the measured  $dN/dy$  of  ${}^4\text{He}$  ( ${}^4\overline{\text{He}}$ ) (i.e., about  $7.8 \pm 3.1 \times 10^{-7}$ ). The larger yields of light (hyper)nuclei at lower colliding energies are also observed in the predictions of thermal models (see, e.g., Ref. [15]). Compared with  ${}^4\text{He}$  ( ${}^4\overline{\text{He}}$ ), the larger or comparable yields of  ${}^4_{\Lambda}\text{H}$  ( ${}^4_{\Lambda}\overline{\text{H}}$ ) are mainly due to the effects of earlier  $\Lambda$  freezeout. Generally, the yields of anti-(hyper)nuclei increase with the colliding energy, and here that RHIC and LHC have the equal  $dN/dy$  of  ${}^4_{\Lambda}\overline{\text{H}}$  is mainly due to the stronger earlier- $\Lambda$ -freezeout effects at RHIC. The future experimental measurement on  ${}^4_{\Lambda}\text{H}$  ( ${}^4_{\Lambda}\overline{\text{H}}$ ) would be very useful to test the idea of earlier (anti-) $\Lambda$  freezeout.

5. *Conclusion.*—The measured yield ratio  ${}^3_{\Lambda}\text{H}/{}^3\overline{\text{He}}$  ( ${}^3_{\Lambda}\overline{\text{H}}/{}^3\overline{\text{He}}$ ) in heavy-ion collisions at RHIC and LHC can be naturally explained by the covariant coalescence model if the (anti-) $\Lambda$  particles freeze out earlier than

(anti-)nucleons but their relative freezeout time is closer at LHC than at RHIC. The earlier (anti-) $\Lambda$  freezeout can significantly enhance the yield of  ${}^4_{\Lambda}\text{H}$  ( ${}^4_{\Lambda}\overline{\text{H}}$ ), leading to that  ${}^4_{\Lambda}\overline{\text{H}}$  provides an easily measured candidate for antimatter heavier than  ${}^4\overline{\text{He}}$ . The larger relative p- $\Lambda$  ( $\overline{\text{p}}-\overline{\Lambda}$ ) freezeout time difference at RHIC leads to a larger (equal) yield of  ${}^4_{\Lambda}\text{H}$  ( ${}^4_{\Lambda}\overline{\text{H}}$ ) at RHIC than at LHC. In future, more precise measurement on  ${}^3_{\Lambda}\text{H}/{}^3\text{He}$  and  ${}^3_{\Lambda}\overline{\text{H}}/{}^3\overline{\text{He}}$  as well as the measurement on  ${}^4_{\Lambda}\text{H}$  and  ${}^4_{\Lambda}\overline{\text{H}}$  would be extremely helpful to test the proposed freezeout scenario for (anti-) $\Lambda$  particles and the predictions on light (anti-)hypernuclei production presented in this work.

*Acknowledgments.*—We are grateful to Vincenzo Greco, Che Ming Ko, Yu-Gang Ma, Zhang-Bu Xu, Zhong-Bao Yin and Xian-Rong Zhou for helpful discussions. This work was supported in part by the Major State Basic Research Development Program (973 Program) in China under Contract Nos. 2015CB856904 and 2013CB834405, the NSFC under Grant Nos. 11275125 and 11135011, the “Shu Guang” project supported by Shanghai Municipal Education Commission and Shanghai Education Development Foundation, the Program for Professor of Special Appointment (Eastern Scholar) at Shanghai Institutions of Higher Learning, and the Science and Technology Commission of Shanghai Municipality under Grant No. 11DZ2260700.

- 
- [1] B. I. Abelev et al. (STAR Collaboration), arXiv:0909.0566.
- [2] H. Agakishiev et al. (STAR Collaboration), *Nature* **473**, 353 (2011).
- [3] N. Sharma (for the ALICE collaboration), *J. Phys. G* **38**, 124189 (2011).
- [4] J. Adam et al. (ALICE Collaboration), *Phys. Rev. C* **93**, 024917 (2016).
- [5] Y. G. Ma, J. H. Chen, and L. Xue, *Front. Phys.* **7**, 637 (2012); *Y. G. Ma, J. Phys.: Conf. Series* **420**, 012036 (2013); *EPJ Web of Conf.* **66**, 04020 (2014).
- [6] J. Adam et al. (ALICE Collaboration), *Nature Phys.* **11**, 811 (2015).
- [7] L. Adamczyk et al. (STAR Collaboration), *Nature* **527**, 345 (2015).
- [8] E. Carlson, A. Coogan, T. Linden, S. Profumo, A. Ibarra, and S. Wild, *Phys. Rev. D* **89**, 076005 (2014).
- [9] W. Greiner, *Int. J. Mod. Phys. E* **5**, 1 (1996); *J. Phys.: Conf. Series* **413**, 012002 (2013).
- [10] K. J. Sun and L. W. Chen, *Phys. Lett. B* **751**, 272 (2015).
- [11] P. Koch, B. Müller, and J. Rafelski, *Phys. Rep.* **142**, 167 (1986).
- [12] C. M. Ko, *Phys. Rev. C* **32**, 326 (1985).
- [13] B. I. Abelev et al. (STAR Collaboration), *Science* **328**, 58 (2010).
- [14] J. Adam et al. (ALICE Collaboration), *Phys. Lett. B* **754**, 360 (2016).
- [15] A. Andronic, P. Braun-Munzinger, J. Stachel, and H. Stöcker, *Phys. Lett. B* **697**, 203 (2011).
- [16] J. Cleymans, S. Kabana, I. Kraus, H. Oeschler, K. Redlich, and N. Sharma, *Phys. Rev. C* **84**, 054916 (2011).
- [17] S. Pal and W. Greiner, *Phys. Rev. C* **87**, 054905 (2013).
- [18] M. Petran, J. Letessier, V. Petracek, and J. Rafelski, *Phys. Rev. C* **88**, 034907 (2013).
- [19] S. Chatterjee and B. Mohanty, *Phys. Rev. C* **90**, 034908 (2014).
- [20] G. Chen, H. Chen, J. Wu, D. S. Li, and M. J. Wang, *Phys. Rev. C* **88**, 034908 (2013).
- [21] Z. She, G. Chen, H. Xu, T. Zeng, and D. Li, arXiv:1509.06493.
- [22] S. Zhang, J. H. Chen, H. Crawford, D. Keane, Y. G. Ma, and Z. B. Xu, *Phys. Lett. B* **684**, 224 (2010).
- [23] L. Xue, Y. G. Ma, J. H. Chen, and S. Zhang, *Phys. Rev. C* **85**, 064912 (2012).
- [24] N. Shah, Y. G. Ma, J. H. Chen, and S. Zhang, *Phys. Lett. B* **754**, 6 (2016).
- [25] E. Botta, T. Bressani, and G. Garbarino, *Eur. Phys. J. A* **48**, 41 (2012).
- [26] C. B. Dover, U. Heinz, and E. Schnedermann, *Phys. Rev. C* **44**, 1636 (1991).
- [27] S. T. Butler and C. A. Pearson, *Phys. Rev. Lett.* **7**, 69 (1961).
- [28] H. Sato and K. Yazaki, *Phys. Lett. B* **98**, 153 (1981).
- [29] L. P. Csernai and J. I. Kapusta, *Phys. Rep.* **131**, 223 (1986).
- [30] J. Cleymans, K. Redlich, and E. Suhonen, *Z. Phys. C* **51**,

- 137 (1991).
- [31] P. Braun-Munzinger and J. Stachel, *J. Phys. G* **21**, L17 (1995); *Nature* **448**, 302 (2007).
- [32] J. Steinheimer, K. Gudima, A. Botvina, I. Mishustin, M. Bleicher, and H. Stöcker, *Phys. Lett. B* **714**, 85 (2012).
- [33] R. Mattiello, H. Sorge, H. Stöcker, and W. Greiner, *Phys. Rev. C* **55**, 1443 (1997).
- [34] L. W. Chen, C. M. Ko, and B. A. Li, *Phys. Rev. C* **68**, 017601 (2003); *Nucl. Phys. A* **729**, 809 (2003); *Phys. Rev. C* **69**, 054606 (2004).
- [35] L. W. Chen and C. M. Ko, *Phys. Rev. C* **73**, 044903 (2006).
- [36] Y. Oh, Z. W. Lin, and C. M. Ko, *Phys. Rev. C* **80**, 064902 (2009).
- [37] L. Zhu, C. M. Ko, and X. Yin, *Phys. Rev. C* **92**, 064911 (2015).
- [38] F. Retière and M. A. Lisa, *Phys. Rev. C* **70**, 044907 (2004).
- [39] G. Röpke, *Phys. Rev. C* **79**, 014002 (2009).
- [40] H. Nemura, Y. Suzuki, Y. Fujiwara, and C. Nakamoto, *Prog. Theor. Phys.* **103**, 929 (2000).
- [41] S. S. Adler et al. (PHENIX Collaboration), *Phys. Rev. C* **69**, 034909 (2004).
- [42] B. Abelev et al. (ALICE Collaboration), *Phys. Rev. Lett.* **109**, 252301 (2012).
- [43] G. Agakishiev et al. (STAR Collaboration), *Phys. Rev. Lett.* **108**, 072301(2004).
- [44] B. Abelev et al. (ALICE Collaboration), *Phys. Rev. Lett.* **111**, 222301 (2013).
- [45] M. He, R. J. Fries, and R. Rapp, *Phys. Rev. C* **82**, 034907 (2010).
- [46] K. A. Bugaev, D. R. Oliinychenko, J. Cleymans, A. I. Ivanytskyi, I. N. Mishustin, E. G. Nikonov, and V. V. Sagun, *Europhys. Lett.* **104**, 22002 (2013).
- [47] S. Chatterjee, R. M. Godbole, and S. Gupta, *Phys. Lett.* **B727**, 554 (2013).
- [48] S. Chatterjee, B. Mohanty, and R. Singh, *Phys. Rev. C* **92**, 024917 (2015).
- [49] L. V. Bravina, K. Tywoniuk, and E. E. Zabrodin, *J. Phys. G* **31**, S989 (2005).
- [50] M. Juric et al., *Nucl. Phys.* **B52**, 1 (1973).
- [51] M. Wang et al., *Chin. Phys. C* **36**, 1603 (2012).
- [52] A. Esser et al. (A1 Collaboration), *Phys. Rev. Lett.* **114**, 232501 (2015).
- [53] T. A. Armstrong et al. (E864 Collaboration), *Phys. Rev. C* **70**, 024902 (2004).
- [54] V. Koch, A. Majumder, and J. Randrup, *Phys. Rev. Lett.* **95**, 182301 (2005).
- [55] C. Rappold et al., *Phys. Lett.* **B728**, 543 (2014).
- [56] I. Kumagai-Fuse, S. Okabe, and Y. Akaishi, *Nucl. Phys.* **A585**, 365c (1995).
- [57] H. Ota, *Nucl. Phys.* **A639**, 251c (1998).
- [58] N. Sharma (for the ALICE Collaboration), *Nucl. Phys.* **A**, (2016), in press [arXiv:1602.02173].